Modelling the high temperature oxidation of titanium alloys: Development of a new numerical tool PyTiOx

Clément Ciszak [a,*], Daniel Monceau [a], Clara Desgranges [b]

[a] CIRIMAT, Université de Toulouse, CNRS, INP-ENSIACET, 4 allée Emile Monso - BP44362, 31030, Toulouse, France
[b] Safran-Tech, Materials and Processes Department, Rue des Jeunes Bois, Châteaufort, 78114, Magny-les-Hameaux, France

Keywords:
A. Titanium
A. Alloy
B. Modelling studies
C. High temperature corrosion

A B S T R A C T

The PyTiOx numerical tool was designed to model the high-temperature oxidation of titanium alloys by solving diffusion equations in a 1D finite size metal/oxide system with a moving metal|oxide interface. Input parameters were selected to investigate Ti6242s alloy oxidation. PyTiOx overcomes certain limitations compared with analytical models, which can study different quantitative effects on both oxide scaling kinetics and oxygen diffusion in the alloy, such as nominal O concentration, thin samples and non-isothermal conditions. It also gives life span estimates. Calculations with non-isothermal conditions revealed the possible existence of a transient, oxide scale reduction regime after a drop in temperature.

1. Introduction

Titanium alloys are widely used in aircraft and helicopter engines for their good strength-to-density ratio. However, they cannot operate at very high temperatures due to their behaviour in such oxidizing conditions. In order to limit operating costs and the ecological impact of air traffic, titanium alloys would need to operate at higher temperatures. This would lead to better engine efficiency which would allow to compete with heavier alloys, such as Ni-based super-alloys. The engineering and scientific challenge consists in improving the resistance of Ti alloys to high-temperature oxidation and oxygen embrittlement, while limiting the deterioration of their specific mechanical properties as temperature increases. It is common knowledge that high-temperature oxidation of Ti alloys leads to the formation of a TiO_2 scale on the surface of the material. Like Zr, Ti has the specific ability to dissolve large amounts of oxygen in its metallic matrix (up to 33 at. % for pure Ti), which also induces the formation of an oxygen diffusion profile delimiting an oxygen affected zone (OAZ). On one hand, this O dissolution decreases the ductility of the affected area, which can lead to structural failure. On the other hand, it increases the mechanical strength and elastic moduli of this area [1,2]. Thus, it appears crucial to predict as accurately as possible the high temperature oxidation behavior of Ti-based components in order to improve sizing and durability estimates. Based on the analytical resolution of Fick's laws, several analytical models have been put forward to predict the shape of oxygen diffusion profiles within materials. Due to intrinsic limitations of these analytical tools, numerical models for the high-temperature oxidation of Zr-alloys have also been developed [3]. To our knowledge however, these numerical approaches have never been applied to Ti alloys.

This paper first describes the analytical models that are commonly used to characterize the high-temperature oxidation of titanium alloys as well as the limitations of these models. Then, the new numerical model – PyTiOx – is described in detail. In the second part of the paper, the calculation results obtained using this numerical model are discussed to study different quantitative effects on the high-temperature oxidation behavior of Ti alloys: nominal O concentration, thin samples and non-isothermal conditions.

2. Analytic modelling of the high-temperature oxidation of Ti alloys

2.1. Brief review of commonly-used analytic models suitable for the high-temperature oxidation of Ti alloys

2.1.1. Modelling oxygen dissolution in the metal

At high temperatures, the oxidation of Ti alloys is known to be controlled by the diffusion of O within both the TiO_2 oxide scale and the Ti metallic substrate [4]. Thus, O concentration profiles in the system (oxide and metal) can be simulated using classic laws of solid state diffusion [5]. Based on the analytical resolution of Fick's laws, several

* Corresponding author.
E-mail address: clement.ciszak@toulouse-inp.fr (C. Ciszak).

https://doi.org/10.1016/j.corsci.2020.109005

analytic models have been proposed to predict O diffusion profiles within materials. From the simple *erf* function which takes into account the diffusion in a single phase [5], to more complete models that take into account the formation of a second phase, i.e. the oxide, and the displacement of the metal|oxide interface [5,6].

During the oxidation of Ti alloys, observations show that O dissolution depth typically reaches about 10 times the oxide scale thickness. Consequently, the metal|oxide interface recession can often be neglected when calculating O diffusion in the metallic matrix. The inward diffusion and dissolution of oxygen in the matrix can therefore be considered as the only phenomenon to be taken into account. Within this framework, the simplest approach to predict the O diffusion profile within the Ti matrix, consists in using a simple *erf* function (Eq. (1)) [5],

$$C_{O\,(Ti)}\,(z,t) = \mathit{erfc}\left(\frac{z}{2\sqrt{D_{O\,(Ti)}t}}\right)\left(C_{Ti|\,TiO_2} - C_0\right) + C_0 \tag{1}$$

where $C_{O\,(Ti)}\,(z,t)$ is the local O concentration (in at. fraction), z represents the distance from the metal|oxide interface (in m), t the time of oxidation (in s), $D_{O\,(Ti)}$ the oxygen diffusion coefficient within the alloy (in $m^2.s^{-1}$), $C_{Ti|\,TiO_2}$ the O concentration (in at. fraction) at the $Ti|TiO_2$ interface in the metal, and C_0 the initial nominal O content (in at. fraction).

2.1.2. Modelling oxygen diffusion in the oxide and the metal

Yet, oxide scale growth and O dissolution are two correlated phenomena and oxide scaling cannot be neglected in the mass balance. A more compete analytic model involving this coupling must therefore be used, such as the solution proposed by Wagner [7] and compiled by Crank [5] for phase transformations. This new model takes into account the displacement of the interface between the two adjacent phases. Applying this model to the case of an oxide layer growing on the surface of a metallic matrix leads to the following diffusion equations in the oxide (Eq. (2)) and in the metal (Eqs. (3) and (4)). The model also defines the metal|oxide interface displacement (Eq. (6)) with the introduction of the γ constant (Eq. (7)). This γ constant, which is relative to the coupling between oxide scale formation and diffusion within the metallic matrix, allows to take into account the effect of this coupling on the metal|oxide displacement kinetics. Even if the γ constant does not have a direct analytical expression, it only depends on the physico-chemical parameters chosen for the model (concentration at interfaces and diffusion coefficients). It is directly linked to the division of the O flux reaching the metal|oxide interface: one part is dissolved in the alloy and the other contributes the oxide scale growth.

$$C_{O\,(TiO_2)}(z_1,t) = C_s - \mathit{erf}\left(\frac{z_1}{2\sqrt{D_{O\,(TiO_2)}t}}\right)\frac{\left(C_s - C_{TiO_2|Ti}\right)}{\operatorname{erf}\gamma} \tag{2}$$

$$C_{O\,(Ti)}(z_2,t) = \mathit{erfc}\left(\frac{z_2}{2\sqrt{D_{O\,(Ti)}t}}\right)\left(\frac{C_{Ti|\,TiO_2} - C_0}{\mathit{erfc}\left(\frac{\gamma\sqrt{\varphi}}{p}\right)}\right) + C_0 \tag{3}$$

$$z_2 = z_1 + \xi(t)\cdot\frac{1-p}{p} \tag{4}$$

$$\varphi = \frac{D_{O\,(TiO_2)}}{D_{O\,(Ti)}} \tag{5}$$

$$\xi(t) = 2\gamma\sqrt{D_{O\,(TiO_2)}t} \tag{6}$$

$$C_{TiO_2|Ti} - \frac{C_{Ti|\,TiO_2}}{p} = \frac{C_s - C_{TiO_2|Ti}}{\gamma\sqrt{\pi}\operatorname{erf}\gamma}\exp\left(-\gamma^2\right) - \frac{\left(C_{Ti|\,TiO_2} - C_0\right)\exp\left(-\frac{\gamma^2\varphi}{p^2}\right)}{\gamma\sqrt{\varphi}\sqrt{\pi}\operatorname{erfc}\left(\frac{\gamma\sqrt{\varphi}}{p}\right)} \tag{7}$$

Here, $D_{O\,(TiO_2)}$ represents the diffusion coefficient of O in the oxide scale (in $m^2.s^{-1}$), φ the ratio of oxygen diffusion coefficients in TiO_2 and in the Ti matrix (Eq. (5)), C_s and $C_{TiO_2|Ti}$ the O content (in at. fraction) in the oxide at the oxide|gas interface and the oxide|metal interface respectively, ξ the oxide scale thickness (in m), p the Pilling and Bedworth ratio (PBR) and γ the coupling constant.

A graphical illustration of Wagner's model is presented in Appendix A.

2.1.3. Modelling finite size samples

In the case of thin samples and long oxidation treatments, O inward diffusion may reach the samples center, resulting in the progressive O saturation of the samples over time. This particular behavior cannot be reproduced by the two previous models in which samples are assumed semi-infinite. Thus, Pawel [6] proposed a semi-analytic model for finite dimension specimens. The new equation describing the O diffusion profile in the Ti matrix is presented in Eq. (8),

$$C_{O\,(Ti)}(z_2,t) = \frac{\left[1 - \frac{1}{2}\theta(z_2)\right]}{\left[1 - \frac{1}{2}\theta\left(\frac{\xi}{p}\right)\right]}\left(C_{Ti|\,TiO_2} - C_0\right) + C_0 \tag{8}$$

where θ, which is a function of x or ξ, is detailed in Eq. (9):

$$\begin{aligned}\theta(z_2) = {} & \left(\operatorname{erf}\frac{h - z_2}{2\sqrt{D_{O(Ti)}t}} + \operatorname{erf}\frac{z_2}{2\sqrt{D_{O(Ti)}t}}\right) + \left(\operatorname{erf}\frac{z_2}{2\sqrt{D_{O(Ti)}t}}\right. \\ & \left. - \operatorname{erf}\frac{h + z_2}{2\sqrt{D_{O(Ti)}t}}\right) + \left(\operatorname{erf}\frac{3h - z_2}{2\sqrt{D_{O\,(Ti)}t}} - \operatorname{erf}\frac{2h - z_2}{2\sqrt{D_{O\,(Ti)}t}}\right) \\ & - \left(\operatorname{erf}\frac{2h - z_2}{2\sqrt{D_{O\,(Ti)}t}} - \operatorname{erf}\frac{h - z_2}{2\sqrt{D_{O\,(Ti)}t}}\right) - \left(\operatorname{erf}\frac{h + z_2}{2\sqrt{D_{O\,(Ti)}t}}\right. \\ & \left. - \operatorname{erf}\frac{2h + z_2}{2\sqrt{D_{O\,(Ti)}t}}\right) + \left(\operatorname{erf}\frac{2h + z_2}{2\sqrt{D_{O\,(Ti)}t}} - \operatorname{erf}\frac{3h + z_2}{2\sqrt{D_{O\,(Ti)}t}}\right)\end{aligned} \tag{9}$$

Here, h represents the initial thickness of the specimen (in m).

Again, a graphical illustration of Pawel's model is presented in Appendix A.

2.2. Input parameters

The equations describing the three models presented above require only six independent input parameters: C_s, $C_{TiO_2|Ti}$, $C_{Ti|TiO_2}$, C_0, $D_{O\,(TiO_2)}$ and $D_{O\,(Ti)}$. Data from the literature were collected in order to compare the results for Ti-6Al-2Sn-4Zr-2Mo-Si alloy obtained experimentally to those calculated using the model.

Values of the oxygen concentration in the oxide at the metal|oxide interface, $C_{TiO_2|Ti}$, were calculated using Kofstad's results [8]. Kofstad demonstrated that, in the chemical equilibrium described by Eq. (10), y was proportional to $P_{O_2}^{-1/6}$ (according to Eq. (11)) at 977 °C for P_{O_2} lower than approximately $5{\cdot}10^{-7}$ atm.

$$TiO_{2\,(s)} \rightleftharpoons TiO_{2-y\,(s)} + \frac{y}{2}O_{2\,(g)} \tag{10}$$

$$y = 2\left(\frac{K}{4}\cdot P_{O_2}^{-1/2}\right)^{1/3} \tag{11}$$

Based on Eq. (11), two parameters are needed to calculate the deviation from stoichiometry of TiO_2 at the oxide|metal interface: the equilibrium constant K and the oxygen equilibrium partial pressure at the oxide|metal interface P_{O_2}, for each temperature considered.

First, values of the equilibrium constant K were extrapolated down to 400 °C from Kofstad's results [8] which were obtained between 977 °C and 1 227 °C.

Table 1
Thermodynamic constants used for P_{O_2} calculations.

Thermodynamic constants	R (J. K^{-1}. mol^{-1})	P^0 (atm)	$\Delta_r H^0_{298\,K}$ (kJ. mol^{-1})	$\Delta_r S^0_{298\,K}$ (J. K^{-1}. mol^{-1})
Values	8.314	1	−944.0 ± 0.8 [9]	−185.3 ± 0.1 [9]

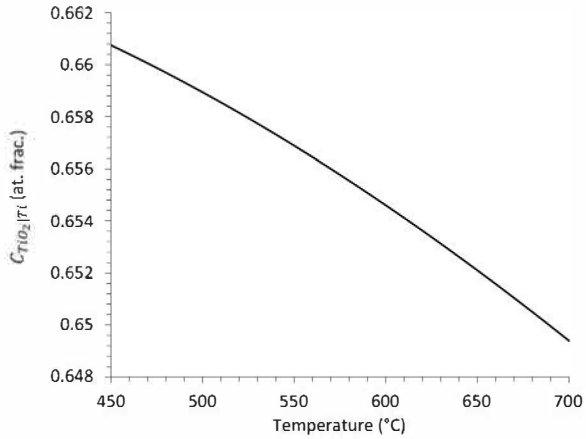

Fig. 1. Evolution of $C_{TiO_2|Ti}$ with temperature.

Table 2
Values of pre-exponential factors and activation energies for O diffusion in TiO_2 and Ti in the case of Ti-6Al-2Sn-4Zr-2Mo-Si alloy from Shenoy *et al.* [11] and Shamblen and Redden [12].

$D^0_{O(TiO_2)}$ (m^2.s^{-1})	$G_{O\,(TiO_2)}$ (kJ. mol^{-1})	$D^0_{O(Ti)}$ (m^2.s^{-1})	$G_{O\,(Ti)}$ (kJ. mol^{-1})
$6.69{\cdot}10^{-2}$ [11]	242.9 [11]	$6.5{\cdot}10^{-5}$ [12]	203 [12]

Second, values of the oxygen equilibrium partial pressure P_{O_2} at the oxide|metal interface were calculated using Ellingham's approximation, following the chemical equilibrium at the oxide|metal interface described in Eq. (12):

$$Ti_{(s)} + O_{2\,(g)} \rightleftharpoons TiO_{2\,(s)} \tag{12}$$

Thus, according to Eq. (12), P_{O_2} can be expressed using the following relationship (Eq. (13)):

$$P_{O_2} = P^0 \cdot \exp\left(\frac{\Delta_r H^0 - T\Delta_r S^0}{RT}\right) \tag{13}$$

where P^0 is the standard pressure (in *atm*), $\Delta_r H^0$ the standard enthalpy of reaction (in $J.mol^{-1}$), $\Delta_r S^0$ the standard entropy of reaction (in $J.K^{-1}.mol^{-1}$), T the absolute temperature (in K) and R the gas constant (in $J.K^{-1}.mol^{-1}$). Literature values of the previous constants [9] that were used for P_{O_2} calculations are given in Table 1. Fig. 1 shows the evolution of $C_{TiO_2|Ti}$ with temperature, calculated using the data in Table 1.

Concerning O diffusion coefficients, Liu and Welsch [10] reported values of pre-exponential factors and activation energies for O diffusion in TiO_2 [11] and in Ti-6Al-2Sn-4Zr-2Mo-Si [12]. These values are presented in Table 2. Data relative to O diffusion in TiO_2 were obtained by fitting the oxide thicknesses measured on samples oxidized in a thermogravimetric apparatus [11]. The parameters, pre-exponential factor $D^0_{O(Ti)}$ and activation energy $G_{O\,(Ti)}$ for O diffusion within the Ti-6Al-2Sn-4Zr-2Mo-Si (Ti6242s) alloy matrix, were calculated from micro-hardness profiles performed on oxidized samples [12]. They are therefore relative to a diffusion process in a two-phase α + β matrix.

In theory, the mass transport of the constituents on a specific sublattice varies with the vacancy site fraction and the site fractions of the constituents. The site fractions depend on the overall composition of the phase, which in turn depends on oxygen activity (see Fig. S1 in Supplementary Materials). The end result is that in the oxide the overall effective mass transport will depend strongly on the oxygen partial pressure, see ref. [13] for a detailed discussion on this subject. For simplification, in the present work, a constant O chemical diffusivity was used to calculate oxygen flux in the oxide scale. The microstructure of the scale may also affect the effective diffusivity in the oxide scale, as has been shown for nickel, iron or chromium oxides [14–16]. However, as long as the contribution of grain boundaries is minor and/or that there is no evolution of the scale microstructure during the oxidation, these effects can be taken into account by considering the kinetics parameter $D_{O\,(TiO_2)}$ as an effective diffusion coefficient in the oxide scale.

2.3. Applying the analytic models to the Ti6242s alloy case

2.3.1. Comparison with experimental data

A first evaluation of results given by these different analytic models, when applied to the high-temperature oxidation of Ti alloys, was performed. Calculated results were compared with experimental findings as regards O diffusion profile, oxide scale thickness and mass gain. Regarding input parameters used for calculations: $C_{TiO_2|Ti}$ was determined with Eq. (11) (its value corresponds to the solubility limit of oxygen in pure Ti), activation energies and pre-exponential factors are given in Table 2. This full set of input parameter values is summarized in Table 3.

Fig. 2 presents the results obtained from the three analytic models detailed above and their comparison with experimental data. These experimental data come from Electron Probe Micro Analysis (EPMA) measurements, cross-section analyses and mass gain measurements performed on Ti-6Al-2Sn-4Zr-2Mo-Si alloy samples oxidized up to 1 000 h at 650 °C in a 80 vol. % Ar / 20 vol. % O_2 gas mixture [17]. From

Table 3
Sets of initial and fitted input parameters respectively based on literature data and fitting of experimental results.

			1st set		2nd set	
Input parameters	General conditions	T (°C)	Imposed	650	Imposed	650
		t (h)		1 000		1 000
	Oxide	C_s (at. %)	Literature values	66.6	Literature values	66.6
		$C_{TiO_2|Ti}$ (at. %)		65.2		65.2
		$G_{O\,(TiO_2)}$ (kJ. mol^{-1})		243 [11]		243 [11]
		$D^0_{O(TiO_2)}$ (m^2.s^{-1})		$6.69{\cdot}10^{-2}$ [11]	Fitted value	$5.4{\cdot}10^{-2}$
	Metal	$C_{Ti|TiO_2}$ (at. %)	Literature values	29.0		22.4
		C_0 (at. %)		0	Fitted values	0.355
		$D^0_{O(Ti)}$ (m^2.s^{-1})		$6.5{\cdot}10^{-5}$ [12]		$2.4{\cdot}10^{-5}$
		$G_{O\,(Ti)}$ (kJ. mol^{-1})		203 [12]	Literature value	203 [12]

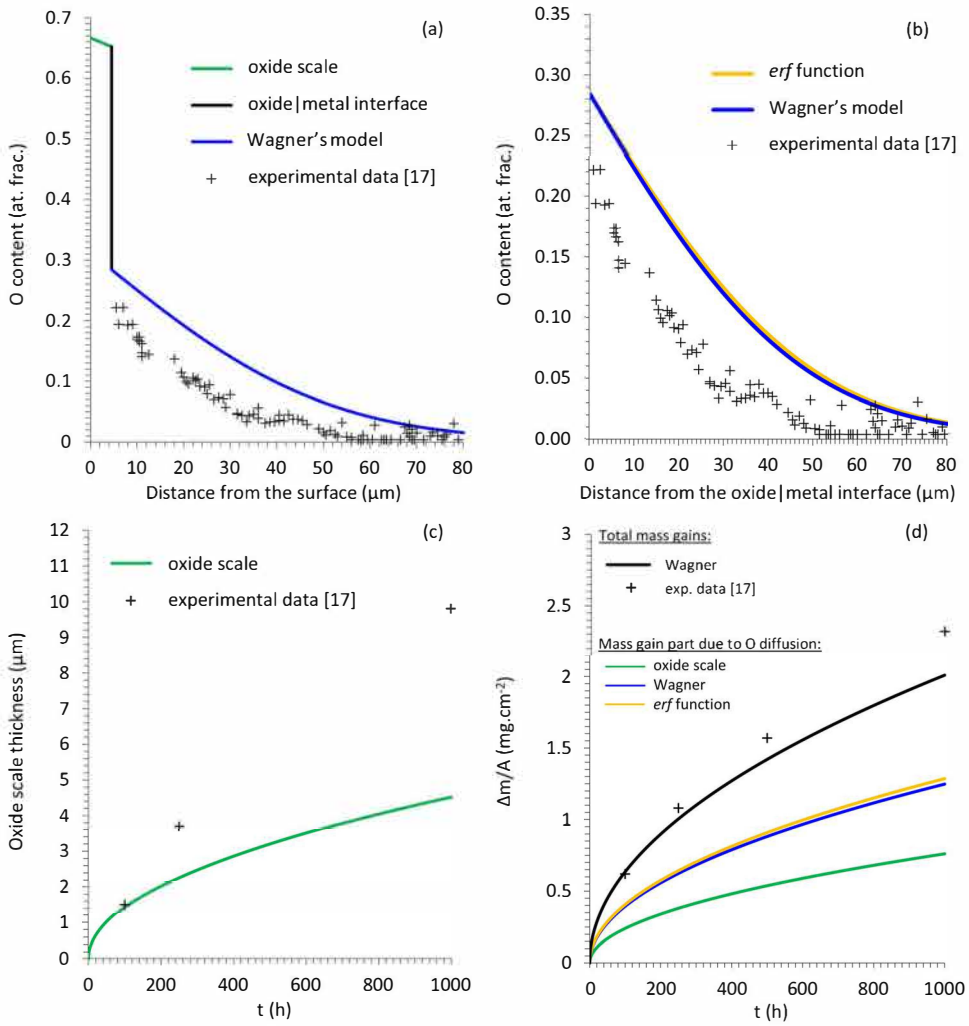

Fig. 2. O profiles (a) and (b), oxide scale thickness (c) and mass gains (d) obtained from analytic models using literature input data, compared with experimental data obtained in a Ti-6Al-2Sn-4Zr-2Mo-Si sample oxidized 1 000 h at 650 °C in a 20 vol. % O_2 / 80 vol. % Ar gas mixture [17].

such specific conditions, it was possible to exclude the formation of nitrides or N-rich α-Ti, which are known to decrease the overall oxidation kinetics [17].

According to Fig. 2, all predictions significantly deviate from experimental data. It is therefore necessary to fit some input parameters with experimental results in order to correctly reproduce the actual behavior of a specimen. This fit was performed through a two-steps method. The first step consisted in fitting some input parameters relative to O diffusion in the metal (namely $C_{Ti|\,TiO_2}$, C_0 and $D^0_{O(Ti)}$) to reproduce as best as possible the O experimental EPMA profile measured in the metal. The second step consisted in fitting the effective diffusion coefficient of O in TiO_2 to reproduce the experimental evolution of the oxide scale thickening as best as possible. The new input parameters obtained after this fitting procedure are presented in Table 3. Calculation results obtained using these data (with fitted values of $C_{Ti|\,TiO_2}$, C_0, $D^0_{O(TiO_2)}$ and $D^0_{O(Ti)}$) are presented in Fig. 3.

According to EPMA data, the O solubility limit should therefore also be fitted to a value close to 22.4 at. %. This lower O solubility, compared that of pure Ti, should first be due to the fact that EPMA measurements of O content are done in an α + β matrix containing 14 vol. % of β, which should dissolve tiny amounts of O. Second, the alloying elements in the α phase may change its O solubility limit. For diffusion coefficients, it was assumed that activation energies were correct, therefore only the values of pre-exponential factors were fitted. As a result, the diffusion coefficient of O in the metallic matrix was divided approximatively by a factor of 2. Such variations in pre-exponential factors might be linked to the chemical composition of the α phase or to a varying contribution of short circuit diffusion paths (i.e. slightly different grain boundary and phase boundary densities) in the overall diffusion process. For either oxide scale or metallic matrix, the magnitude of short circuit diffusion is directly linked to microstructure (e.g. grain size, volume fraction of phases, phases distribution, etc.) and composition (e.g. phases compositions, segregation of impurity at grain boundaries, etc.). Finally, the value of C_0 was updated to correspond to the nominal content of O in the alloy determined by Glow Discharge Mass Spectroscopy (GDMS) [18].

With this second set of input parameters, despite a slight overestimation, the O profile given by the first model (simple *erf* function) appears to be similar to the one obtained from the two other more complete models (Wagner's model and Pawel's model).

The high-temperature oxidation of Ti alloys leads to a high proportion of dissolved oxygen in the metal (nearly 25 at. %) that contributes significantly to the overall mass gain measured experimentally. It is also worth noticing that, unlike the simple *erf* function, Wagner's and Pawel's models enable the direct comparison of calculations with experimental kinetics in terms of mass gain. From Wagner's and Pawel's models it is also possible to calculate separately each medium's (i.e. oxide and metal) contribution to the overall mass gain. Numerical calculations as well as experimental studies confirm that none of these two mass gain contributions can be neglected (25 % in the metal versus 75 % in the oxide in the present case). These values are in agreement with

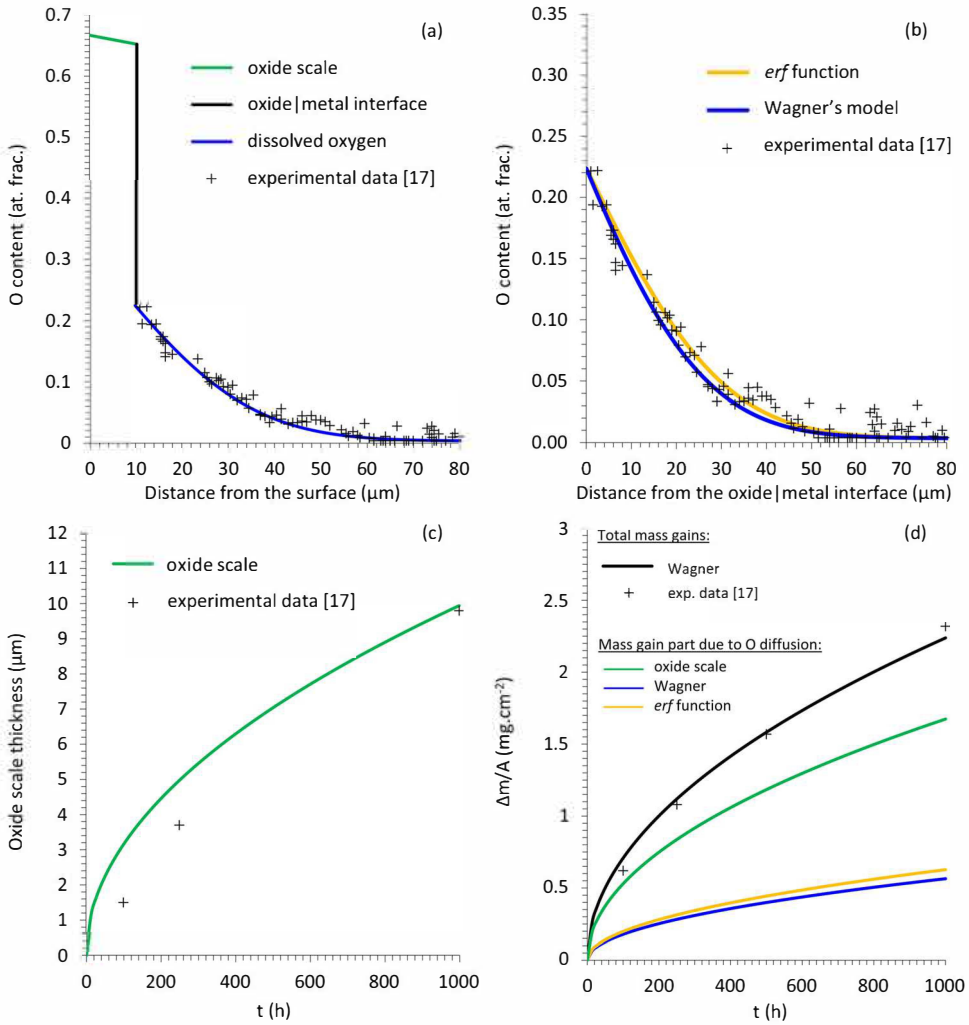

Fig. 3. O profiles (a) and (b), oxide scale thickness (c) and mass gains (d) obtained from analytic models using input parameters adjusted to experimental data obtained in a Ti-6Al-2Sn-4Zr-2Mo-Si sample oxidized 1 000 h at 650 °C in a 20 vol. % O_2 / 80 vol. % Ar gas mixture [17].

those that can be extracted from the results of Dupressoire *et al.* [17] (28 % in the metal versus 72 % in the oxide) after 1 000 h of oxidation under the same conditions.

2.3.2. *Influence of the nominal O content*

Since Wagner's and Pawel's models take into account the coupling between oxide scaling and diffusion within the metallic matrix, they can therefore provide the theoretical evolution of oxide scaling kinetics as a function of initial O content in the metal. For structural applications, OAZ thickness appears more critical than oxide scale thickness, because of its role in crack initiation.

Thus, being able to predict the evolution of OAZ thickness over time as accurately as possible appears to be of major interest when sizing structural components. According to Shamblen and Redden [12], a ductile to non-ductile transition occurs in the Ti-6Al-2Sn-4Zr-2Mo-Si alloy when the local O content exceeds 0.5 at. %. Consequently, the present work refers to the OAZ as the metal thickness whose oxygen content is greater than or equal to 0.5 at. %.

Fig. 4 presents a study of the influence of nominal O concentration on the evolution of OAZ and oxide scale thicknesses over time, using Wagner's model, for 1 000 h long oxidation tests. Calculations were performed for several temperatures ranging from 450 °C to 700 °C and for different initial O contents ranging from 0 to 0.5 at. % (5 000 at. ppm). The value of 0.15 at. % (1 500 at. ppm) corresponds to the nominal O content in pure Ti [19], whereas the value of 0.45 at. % (4 500 at. ppm) is the maximum nominal O content in commercial Ti-6Al-2Sn-4Zr-2Mo-Si alloy [20]. All input parameters used for Fig. 4 calculations are summarized in Table 4.

OAZ thickening kinetics increases significantly with the initial O content for the nominal O concentrations explored, i.e. from 0.15 at. % to 0.45 at. % [20] (Fig. 4a). Given the OAZ definition chosen – the part of the alloy with an oxygen concentration greater than 0.5 at. %. – this result was expected. Oxide scale growth kinetics however, is only slightly affected by the initial O content. It is worth noticing that this method also provides a means to anticipate the life span of a component based on the level of O impurity of the alloy batch. In the rest of the study, it will be assumed that beyond a relative OAZ thickness of approximately 10 % of the overall component thickness, the life span of the component falls down to zero. Based on such a criterion, an attempt was made to evaluate the life span evolution of a 1 mm thick component made of Ti-6Al-2Sn-4Zr-2Mo-Si alloy as a function of both initial O content and temperature.

Fig. 4b presents the life span evolution as a function of initial O content at 650 °C. In the range of nominal O content typically found in industrial alloys, i.e. from 0.15 at. % to 0.45 at. %, calculations show that the life span of the component would almost be halved, before drastically falling down to zero when O content comes close to 0.5 at. %. This type of calculations could be of major interest for the development of additive manufacturing. Indeed, most additive manufacturing processes recycle metal powders left over from prior build cycles. These

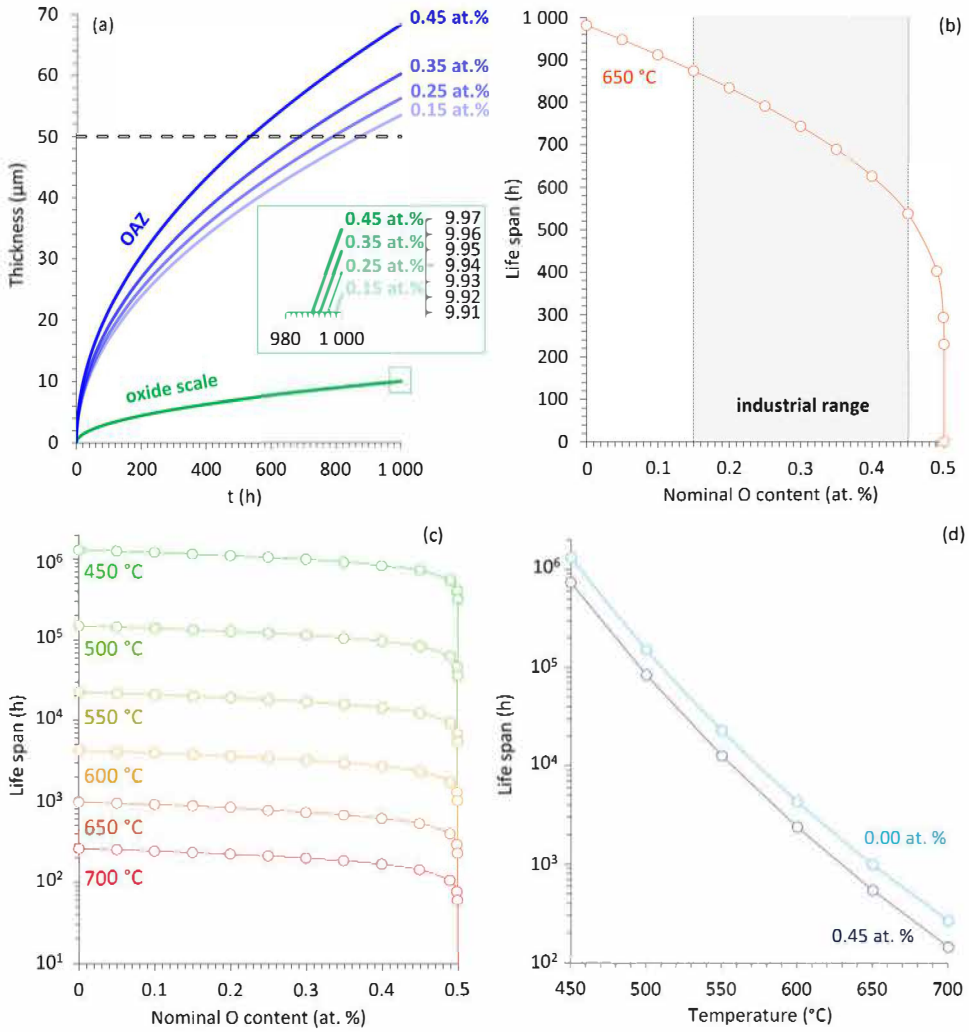

Fig. 4. Evolution of OAZ and oxide scale thicknesses over time calculated for four nominal O contents at 650 °C for a sample with an initial thickness of 1 mm (a), evolution of the life span (see definition in the text) as a function of the nominal O content at 650 °C (b) and for different temperatures ranging from 450 °C to 700 °C (c), evolution of the life span with temperature of a material containing 0.45 at. % of O and an O free material (d).

Table 4
Set of input parameters used to evaluate life spans at 650 °C of a component as a function of its initial content in O.

Input parameters	$C_{TiO_2\|Ti}$ (at. %)	C_s (at. %)	$C_{Ti\|TiO_2}$ (at. %)	C_0 (at. %)	$D^0_{O(TiO_2)}$ ($m^2.s^{-1}$)	$G_{O(TiO_2)}$ (kJ. mol^{-1})	$D^0_{O(Ti)}$ ($m^2.s^{-1}$)	$G_{O(Ti)}$ (kJ. mol^{-1})
Values	$f(T)$ from Eq. (11)	66.6	22.4	0 → 0.5	$5.4{\cdot}10^{-2}$	243 [11]	$2.4{\cdot}10^{-5}$	203 [12]

powders are therefore progressively enriched in oxygen over the successive cycles.

As expected, temperature is the parameter that most affects life span, as shown in Fig. 4c and d. Indeed, although the O content (industrial range) can halve the component's life span, a temperature decrease of 50 °C reduces the life span of about one order of magnitude.

2.3.3. *Behavior of thin components*

In order to reduce the mass of certain components, hollow structures made of thin parts are often used. However, thin samples do not behave like massive samples in terms of diffusion. The model proposed by Pawel aims at anticipating this phenomenon. A quantitative application was proposed in a previous work [21]. The calculations were performed on a 100 µm thick sample. The same calculations are updated here using the fitted parameters (2nd set) presented in Table 3 for oxidations at 650 °C for 73 000 h.

Fig. 5 presents calculation results of O diffusion profiles in the metallic matrix, total mass gain per unit area and its contributions (oxide growth and O dissolution) as a function of the square root of time.

As can be seen in Fig. 5a, both mass gains per unit area (related to oxide scale formation and O dissolution), appear to follow parabolic kinetics during the first part of the experiment (until 400 h approximately). However, O dissolution kinetics noticeably deviates from this parabolic behavior in the second part of the experiment. This phenomenon is attributed to the progressive oxygen saturation of the metallic matrix and its subsequent consumption by the oxide growth (see Fig. 5b). Indeed, as the metal saturates, the inward O flux progressively decreases as the metal saturates (due to the O concentration gradient decreasing), down to zero upon reaching saturation. Eventually, no more O gets into the metal while the oxide scale keeps growing. The O dissolved in the metal is then transferred to the oxide through the oxidation of the substrate, leading therefore to a decrease in the associated mass gain.

However, despite the fact that both oxide growth and O dissolution

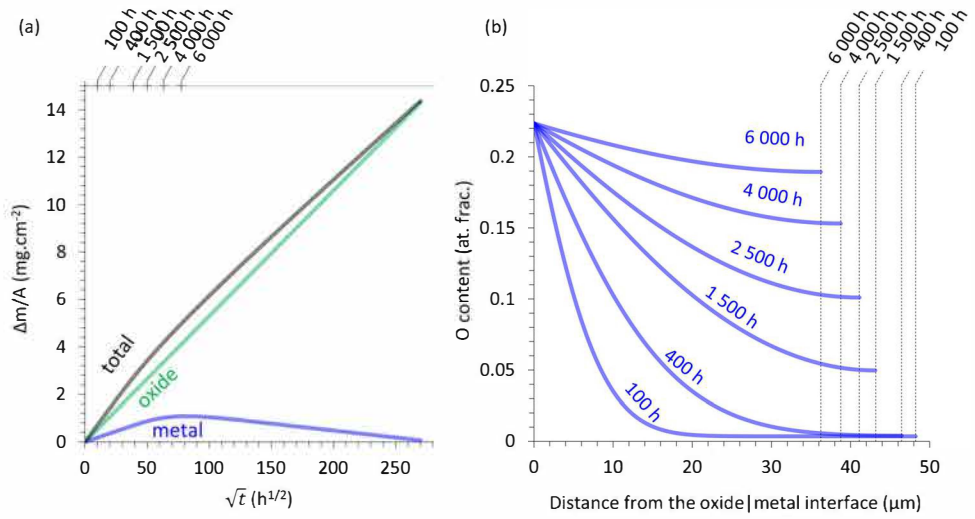

Fig. 5. Evolution of calculated mass gains with the square root of time for a sample of 100 µm initial thickness according to calculations with Pawel's model for 73 000 h of oxidation at 650 °C (a) and evolution of the O diffusion profile within the metallic matrix (progressively consumed by the oxide growth) for the same sample (b).

are correlated phenomena, it is worth noticing that Wagner's and Pawel's models do not predict any feedback effect on the oxide scaling kinetics. Wagner's and Pawel's models predict no evolution of the mass gain kinetics related to the oxide growth when decreasing the sample thickness, although a strong difference appears for the metal part evolution (Fig. 5a). The explanation of such a behavior lies in Eq. (7), from which the value of γ is extracted. Indeed, the primary mathematical problem was established for initial and boundary conditions assumed constant, including parameter C_0. However, for a sample with finite dimensions, C_0 will eventually increase over time, when the O diffusion profile reaches the middle of the sample and until total saturation of the metal (defined by $C_{Ti|TiO_2}$). Consequently, this should inevitably impact the associated value of γ, which describes scale growth kinetics. Pawel's model does not take into account the influence of this evolution to estimate the γ parameter. As a result, although this model was designed to take into account the effect of a finite size sample on the O diffusion in the metal, it does not consider the influence of oxygen saturation in the metal on oxide scaling kinetics. Hence none of these analytic models provide an accurate analysis of the oxidation of thin samples.

First, analytic models suffer from limitations for application cases in which oxidation conditions (time and temperature) lead to an O diffusion profile that will not reach the middle of the sample. Second, the analytical models cannot take into account temperature transients, local evolution of diffusion coefficients, local evolution of the volume fractions of phases and redistribution in the alloying elements, which can be key factors in certain applications. With the objective of mitigating these limitations, numerical approaches were developed.

3. Numerical modelling of the high-temperature oxidation of Ti alloys

Most numerical models involving O dissolution have been developed for high-temperature oxidation of Zr-alloy claddings used in the nuclear industry. Similar approaches can be adapted to Ti alloys. In the next section, after a short review of the existing models, a numerical tool called PyTiOx, which was designed to model the oxidation of titanium alloys, is detailed.

3.1. Available numerical tools

A few numerical tools have been developed over the years to model the high-temperature oxidation of metals. Among them, FROM [22], SVECHA [23], DIFFOX [24], and EKINOX-Zr [13,25] can be cited as numerical models dedicated to the high-temperature oxidation of Zr-alloys. They all use finite differences algorithms based on the solving of Fick's laws in a 1D system that is considered either in Cartesian coordinates [22,25] or in cylindrical coordinates [23,24]. All of them support interface displacements. However, they differ in several aspects. On one hand, only the SVECHA and FROM models allow for O interfacial concentrations to be out of the thermodynamic equilibrium. On the other hand, the DIFFOX and the EKINOX tools support multi-phased materials, such as a stratified oxide scale or a two-phase metallic matrix.

Another numerical method, based on a finite volume method, was proposed by Kitashima *et al.* [26] to model the high-temperature oxidation of α-Ti under isothermal conditions. This model also supports the displacement of the oxide|metal interface, but the rate of the

Table 5
Initial and boundary conditions set for the oxide and metal media.

Medium	Index	Abscissa	Initial conditions	Boundary conditions
Oxide	$i = 1$	$z = z^i$	$x_O(z, t = t_0) = C_s$	$x_O(z, t > 0) = C_s$
	$\forall i \in [1; n]$	$z = z^i + \frac{z^{i+1} - z^i}{2}$	$x_O^i(z, t = t_0) = C_s - erf\left(\frac{z}{2\sqrt{D_{O(TiO_2)}t}}\right)\frac{(C_s - C_{TiO_2\|Ti})}{\mathrm{erf}\gamma}$	/
	$i = n+1$	$z = z^i$	$x_O(z, t = t_0) = C_{TiO_2\|Ti}$	$x_O(z, t > 0) = C_{TiO_2\|Ti}$
	$j = m$	$z = z^j$	$x_O(z, t = t_0) = C_{Ti\|TiO_2}$	$x_O(z, t > 0) = C_{Ti\|TiO_2}$
Metal	$\forall j \in [m; m+q-1]$	$z = z^j + \frac{z^{j+1} - z^j}{2}$	$x_O^j(z, t = t_0) = erfc\left(\frac{z}{2\sqrt{D_{O(Ti)}t}}\right)\left(\frac{C_{Ti\|TiO_2} - C_0}{erfc\left(\frac{\gamma\sqrt{\varphi}}{p}\right)}\right) + C_0$	/
	$j = m+q$	$z = z^j$	$J_O(z, t = t_0) = 0$	$J_O(z, t > 0) = 0$

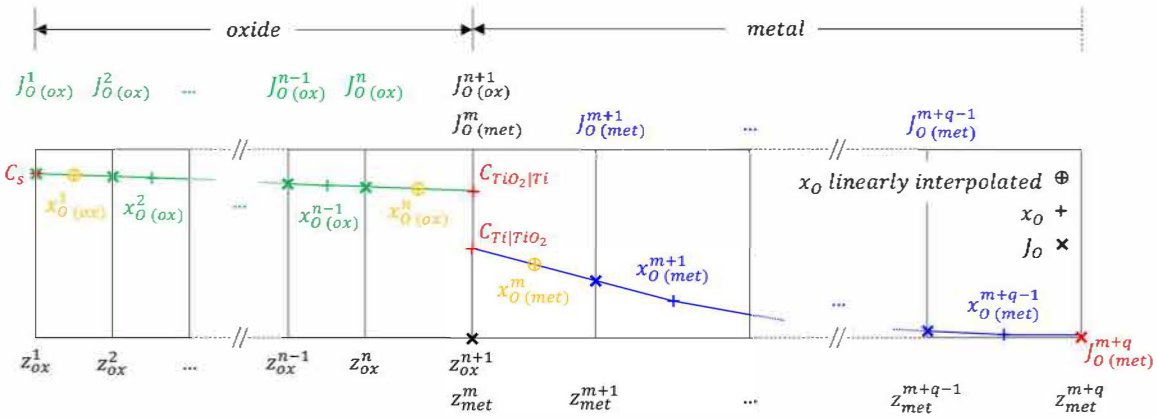

Fig. 6. Schematic representation of the system configuration in the PyTiOx model.

interface recession is calculated from an experimental law accounting for the oxide scale growth kinetics. Therefore, Kitashima's model allows for the oxygen diffusion profiles within the metal to be calculated with the evolution of the oxygen content at the metal|oxide interface over time and with temperature, but it does not take into account the feedback effect previously mentioned, i.e. the influence on scaling kinetics of oxygen dissolution in the metal. The present work aims at developing the same kind of approach proposed for Zr-alloys, but applied to the specific case of high-temperature oxidation of Ti alloys.

3.2. Development of a new numerical tool: PyTiOx

A new numerical tool called PyTiOx was developed based on the numerical scheme of explicit finite differences applied to a 1D calculation domain. The system is composed of two media: one corresponding to the metal and the other to the oxide scale with an initial thickness of ξ_0, which is taken as small as possible to simulate the oxidation of an initially unoxidized alloy. The two media are treated separately. Each medium is divided into slices: the oxide into n slices and the metal into q slices. The meshes of the oxide and of the metal are anchored in their respective crystallographic lattice. Therefore, the slices inside the oxide and inside the metal do not move relative to the oxide and metal lattices respectively, but the oxide and metal meshes move relative to each other. A moving interface algorithm enables to describe the growth/thinning of the oxide scale and the corresponding metal recession/growth.

The O concentration in each slice "i" is designated as $x^i_{O\,(medium)}$. Table 5 presents the initial and boundary conditions set for the oxide and the metal media. The boundary conditions used for the following application of the numerical model are the same as those chosen in Wagner's analytical model for the concentration at oxide surface (C_s) and at the metal|oxide interface ($C_{TiO_2|Ti}$ and $C_{Ti|TiO_2}$). As in Wagner's model, these two interfaces are considered to be at the local equilibrium. To integrate finite size samples, the boundary condition at the last metal slice on the right side, i.e. the center of the sample, is a null flux ($J_O\,(z = z^{m+q}, t > 0) = 0$). According to Eqs. (6) and (7), the actual initial time t_0 is recalculated based on the oxide thickness ξ_0 initially set, so that the thickness of the oxide and of the OAZ have a value of 0 at time $t = 0$. This value of t_0 is then used to calculate the corresponding initial oxygen diffusion profile in each medium, using Eqs. (2) and (3) for the oxide and the metal, respectively.

Fig. 6 presents a schematic representation of the system configuration. Values of boundary conditions presented in Table 5 can only change with temperature. They were therefore considered constant in the calculations under isothermal conditions.

At each time step Δt, O transport between slices is calculated using O fluxes, J_O, from the following equations (Eqs. (14)–(16)):

$$\text{For } i = 1 \;:\; \left(J^i_{O\,(ox)}\right)_t = -D_{O\,(ox)} \frac{\left(x^i_{O\,(ox)}\right)_t - C_s}{\frac{1}{2}\left(z^{i+1}_{(ox)} - z^i_{(ox)}\right)_t} \tag{14}$$

$$\forall i \in]1;n] \;:\; \left(J^i_{O\,(ox)}\right)_t = -D_{O\,(ox)} \cdot \left(\frac{x^i_{O\,(ox)} - x^{i-1}_{O\,(ox)}}{\frac{1}{2}\left(z^{i+1}_{(ox)} - z^{i-1}_{(ox)}\right)} \right)_t \tag{15}$$

$$\forall j \in [m+1;m+q-1] \;:\; \left(J^j_{O\,(met)}\right)_t = -D_{O\,(met)} \cdot \left(\frac{x^j_{O\,(met)} - x^{j-1}_{O\,(met)}}{\frac{1}{2}\left(z^{j+1}_{(met)} - z^{j-1}_{(met)}\right)} \right)_t \tag{16}$$

The flux balance, performed for each slice using the fluxes previously determined at time t, allows for the explicit treatment of the O mass balance in each slice at time $t + \Delta t$, according to the following relationships (Eqs. (17) and (18)):

$$\forall i \in [2;n-1] \;:\; \left(x^i_{O\,(ox)}\right)_{t+\Delta t} = \left(x^i_{O\,(ox)} + \frac{J^i_{O\,(ox)} - J^{i+1}_{O\,(ox)}}{z^{i+1}_{(ox)} - z^i_{(ox)}} \right)_t \cdot \Delta t \tag{17}$$

$$\forall j \in [m+1;m+q-1] \;:\; \left(x^j_{O\,(met)}\right)_{t+\Delta t} = \left(x^j_{O\,(met)} + \frac{J^j_{O\,(met)} - J^{j+1}_{O\,(met)}}{z^{j+1}_{(met)} - z^j_{(met)}} \right)_t \cdot \Delta t \tag{18}$$

The algorithm for the displacement of the metal|oxide interface relies on the growth and thinning of the slice of each medium that is adjacent to the metal|oxide interface. The algorithm of growth and thinning is based on a mass balance considering fixed concentrations at the metal|oxide interface $C_{Ti|TiO_2}$ and $C_{TiO_2|Ti}$. Assuming a linear interpolation of the O concentration profile in the first slice of each medium adjacent to the metal|oxide interface, the total O quantity $Q_{O\,(tot)}$ present in the slices "n" and half of "$n-1$", "m" and half of "$m+1$" can be expressed as follows:

$$\left(Q_{O\,(tot)}\right)_t = \left(Q_{O\,(ox)} + Q_{O\,(met)}\right)_t \tag{19}$$

With:

$$\left(Q_{O\,(ox)}\right)_t = \left(\frac{1}{2}\left(C_{TiO_2|Ti} + x^{n-1}_{O\,(ox)} \right) \left(\Delta z^n_{ox} + \frac{\Delta z^{n-1}_{ox}}{2} \right) \right)_t \tag{20}$$

$$\left(Q_{O\,(met)}\right)_t = \left(\frac{1}{2}\left(C_{Ti|TiO_2} + x^{m+1}_{O\,(met)} \right) \left(\Delta z^m_{met} + \frac{\Delta z^{m+1}_{met}}{2} \right) \right)_t \tag{21}$$

$$\forall i \in [1;n] \;:\; \Delta z^i_{ox} = z^{i+1}_{ox} - z^i_{ox} \tag{22}$$

$$\forall j \in [m;m+q-1] \;:\; \Delta z^j_{met} = z^{j+1}_{met} - z^j_{met} \tag{23}$$

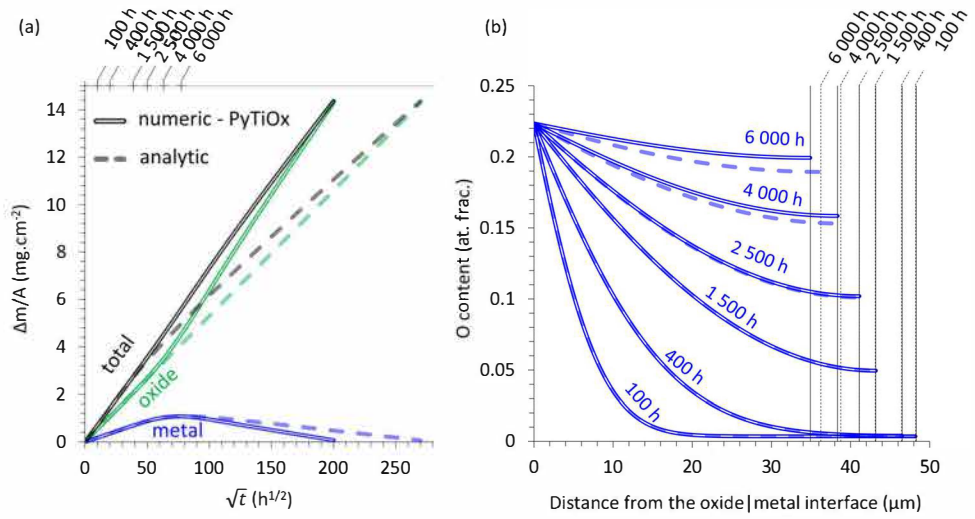

Fig. 7. Comparison of the evolution of numerically and analytically (Fig. 5) calculated mass gains as a function of the square root of time for a 100 μm thick sample using Pawel's and PyTiOx models for 73 000 h of oxidation at 650 °C (a) and evolution of the O diffusion profiles within the metallic matrix (progressively consumed by the oxide growth) relative to a 100 μm thick sample (b).

Then, considering the mass balance from O fluxes getting in the last oxide slice and a half adjacent to the metal|oxide interface, and out of the first metal slice and a half adjacent to the metal|oxide interface:

$$(\Delta Q_O)_t = \left(J_{O\,(ox)}^{TiO_2|Ti} - J_{O\,(met)}^{Ti|TiO_2}\right)_t \cdot \Delta t \tag{24}$$

With $J_{O\,(ox)}^{TiO_2|Ti}$ and $J_{O\,(met)}^{Ti|TiO_2}$, the oxygen fluxes in the middle of the slices $n-1$ and $m+1$, respectively:

$$J_{O\,(ox)}^{TiO_2|Ti} = \frac{J_{O\,(ox)}^{n} + J_{O\,(ox)}^{n-1}}{2} \tag{25}$$

$$J_{O\,(met)}^{Ti|TiO_2} = \frac{J_{O\,(met)}^{m+1} + J_{O\,(met)}^{m+2}}{2} \tag{26}$$

At each time step, the displacement of the metal|oxide interface results from the change in size of the slices that are on each side of the interface.

The size of the metal and oxide slices that are next to the interface are calculated from the oxygen mass balance using Eqs. (19)–(26), and using the mass conservation of Ti, which imposes the following relationship (Eq. (27)):

$$\Delta z_{ox\,(t+\Delta t)}^{n} - \Delta z_{ox\,(t)}^{n} = p\left(\Delta z_{met\,(t)}^{m} - \Delta z_{met\,(t+\Delta t)}^{m}\right) \tag{27}$$

Eq. (27) links the change in size of the oxide and metal slices that are on each side of the interface to the PBR of Ti/TiO_2, i.e. the ratio of the molar volume of Ti in the metal to the molar volume of Ti in the oxide.

In order to minimize calculation errors due to large slices, the displacement of the metal|oxide interface is also modelled by an algorithm that creates or deletes slices in each medium, on both sides of the interface. A growing slice exceeding $\frac{3}{2}\Delta z^0$ is split into two new slices: a first one of Δz^0 thickness and a second one of the remaining thickness. Analogously, a thinning slice becoming thinner than $\frac{1}{2}\Delta z^0$ is merged with the adjacent slice of the same medium (where Δz^0 is the initial thickness of the slices).

This algorithm allowing to solve the moving boundary problem is the same as the one used in several previous works for various simulations with multicomponent diffusion-controlled reaction under local equilibrium. These works concern the kinetic demixing of an oxide solid solution [27], phase transformation under transmutations studies [28], Zr alloys oxidation studies [3,13,25,29] and chromino-former Ni-base

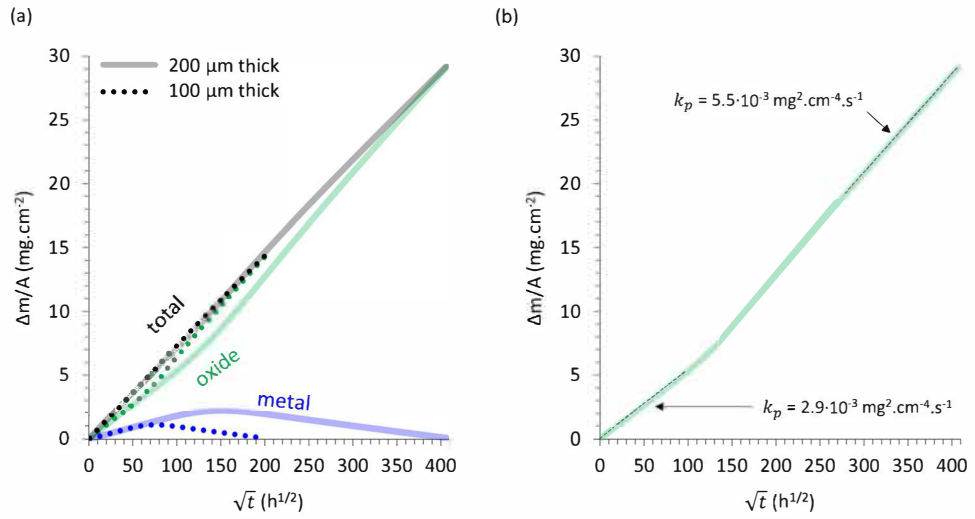

Fig. 8. Overlay of the calculated mass gains per unit area using the PyTiOx model for the oxidation of two different sample sizes (100 μm and 200 μm thick) at 650 °C (a) and focus on the two successive parabolic regimes forming the oxide growth kinetics curve (b).

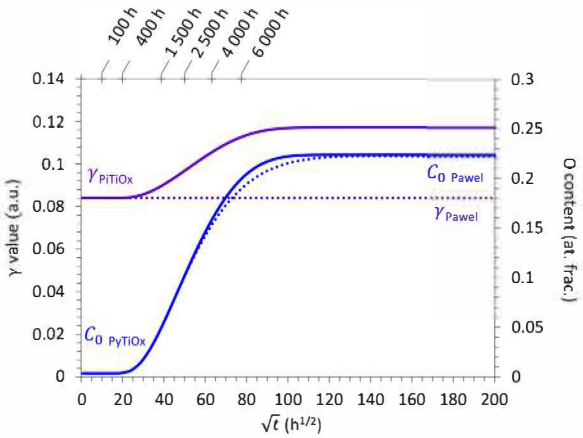

Fig. 9. Evolution of γ and C_0 over time calculated from Pawel's and PyTiOx models for a 100 µm thick sample.

alloys alloy oxidation studies [15,30–32]. This algorithm is perfectly adapted to the explicit finite differences time integration algorithm. A convergence study was performed prior to first calculations allowing to correctly choose the time and space calculation steps (0.857 s for the time calculation step and 0.5 µm and 0.1 µm for space calculation steps in metal and oxide respectively). The algorithm was tested and it correctly reproduces analytical solutions when they exist (See Fig. S2 in the Supplementary Materials). Other works, such as [33], propose different algorithms with an interfacial region that extends to the same depth for both phases. These algorithms also seem to be efficient for various simulations of diffusion-controlled reactions under local equilibrium conditions. In this latter work however, the variation of the molar volume between the two phases is not explicitly taken into account in the moving equation. This cannot be neglected in the case of oxidation which involves important volume changes and where both diffusion in the metal and in the oxide had to be treated. A third solution could be to use the new Sharp Phase Field Method, described by Finel *et al.* [34]. This would also be more efficient in terms of calculation time. However, the explicit finite difference algorithm together with the moving boundary algorithm described here were well suited to the simulations presented in this study.

3.3. PyTiOx results

This section presents the results obtained from PyTiOx calculations for different real-cases applications. The aim is to study quantitatively the influence of sample size (thin wall component) and thermal transient on the behavior of titanium alloys in high-temperature oxidizing conditions.

3.3.1. Sample size effect

Fig. 7 illustrates the calculations performed using the PyTiOx model on a thin, 100 µm thick sample, oxidized 73 000 h at 650 °C. The input data are the same as those used for the calculations performed previously for the same conditions (summarized in Table 3 set 2) using Pawel's analytical model (Fig. 5). The results from Pawel's and PyTiOx models are overlaid to be compared.

PyTiOx calculations show that the growth kinetics of the OAZ and of the oxide scale are both affected by the progressive oxygen saturation of the metal, which occurs at longer durations. The oxide scale growth kinetics appears to be higher than its initial parabolic growth rate. According to Fig. 8a, the thinner the sample is, the earlier this deviation happens. It appears at about 400 h and 20 000 h for 100 µm and 200 µm thick samples, respectively. In agreement with Fig. 7b, this occurs when the metal becomes saturated in O, evidencing a kinetic transition. Indeed, contrary to analytical models, this numerical model accounts for the feedback of the O content evolution at the center of the sample (C_0) on the oxide scaling kinetics. The scaling kinetics of thin samples thus follows two successive regimes. The first one is effective for short oxidation times and is limited by the diffusion of O in both the oxide and the metal. According to Fig. 7a and b, the second one becomes effective once the metal reaches oxygen saturation. At this stage, the O fluxes in the metal decrease to zero, because the O concentration gradient in the metal tends towards zero. Therefore, the entire O flux within the oxide scale is consumed to grow the oxide scale. This is corroborated by Fig. 7a. The oxide scale growth kinetics switch from a first parabolic regime to a second, faster one (Fig. 8b). During the first parabolic regime, the scaling kinetics is controlled by the oxygen flux trough the oxide scale minus the oxygen flux transferred to the metal. During the second one, the scaling kinetics is controlled by the entire oxygen flux crossing the oxide scale and reaching the oxide|metal interface.

Fig. 9 presents the evolution of the O content (C_0) over time at the center of a 100 µm thick sample, provided by both analytical (Pawel's model) and numerical (PyTiOx model) resolutions. The corresponding values of the γ parameter, which describes scale growth kinetics, is also shown. In the PyTiOx model, γ values are calculated using Eq. (7) at each time step. Three stages can be distinguished. The first stage, defined by the first dwell of each curve, corresponds to the parabolic oxidation kinetics of a semi-infinite material containing a nominal O content, C_0. The beginning of the second stage occurs when C_0 starts increasing. It corresponds to a kinetic transition which is directly linked to the evolution of the γ parameter. In the present case, an increase in the scaling kinetics is observed concomitantly with the increase in C_0 and γ, according to PyTiOx results. A third stage then appears once C_0 reaches its maximum value, which corresponds to $C_{Ti|TiO_2}$: the O solubility limit of the material. Hence the scaling kinetics (i.e. the oxide growth) follows a parabolic growth during a first stage, then a transitory stage toward a second accelerated parabolic growth rate (second dwell with constant value for γ). The deviation of the results calculated using Pawel's model from those calculated using the numerical model is evidenced in Fig. 7 and shows the limits of application of this analytical model.

3.3.2. Thermal transient

All the previous numerical and analytical calculations were done in isothermal conditions. However, real in-service conditions involve at least two temperature transients, corresponding to the heating and cooling steps of materials. Most industrial high-temperature equipment is thermally cycled. Analytical models are not suitable for such non-isothermal cases. The numerical model PyTiOx is however able to integrate non-isothermal conditions.

A complex temperature transient, schematically close to the real operating conditions undergone by a component in an aircraft engine made of Ti-alloy, was selected to evaluate the relative contribution of each temperature segment on the overall oxidation process. The input parameters for this calculation are summarized in Table 6.

To avoid excessively long computing times, the lowest temperature was set to 250 °C, assuming that contributions at lower temperatures can

Table 6
Set of input parameters used for calculations in non-isothermal conditions ("~" means that the values of the corresponding parameter vary).

Input parameters	T (°C)	t (h)	h (m)	C_s (at. %)	$C_{TiO_2\|Ti}$ (at. %)	$C_{Ti\|TiO_2}$ (at. %)	C_0 (at. %)	$D^0_{O(TiO_2)}$ ($m^2.s^{-1}$)	$G_{O(TiO_2)}$ (kJ.mol^{-1})	$D^0_{O(Ti)}$ ($m^2.s^{-1}$)	$G_{O(Ti)}$ (kJ.mol^{-1})
Values	~	33000	$1{\cdot}10^{-3}$	66.6	66.5 - 65.5	22.4	0.355	$5.4{\cdot}10^{-2}$	243 [11]	$2.4{\cdot}10^{-5}$	203 [12]

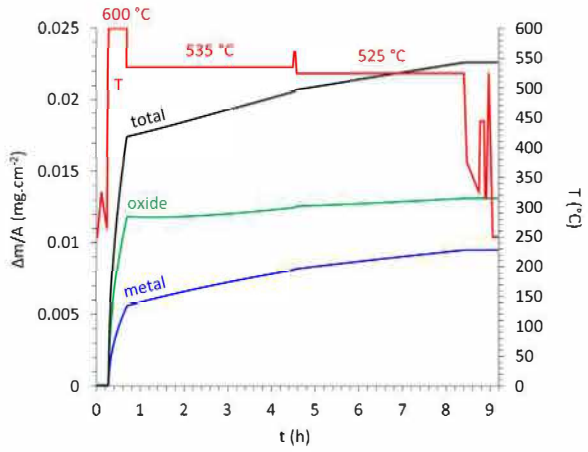

Fig. 10. Evolution of mass gains per unit area over time in non-isothermal conditions.

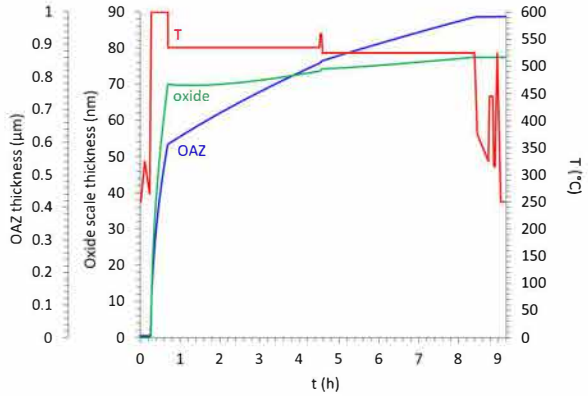

Fig. 11. Evolution of oxide scale and OAZ thicknesses over time in non-isothermal conditions.

be neglected. Fig. 10 presents the evolution of the different mass gains per unit area over time and temperature. In the present case, the material's oxidation behavior appears to be significantly influenced only during the three high-temperature dwells at 600 °C, 535 °C and 525 °C. Despite a few additional variations during the overall thermal transient, the magnitude and/or duration of these thermal variations seem to be too low to significantly influence the oxidation behavior of the sample.

Fig. 11 presents the evolution of oxide scale and OAZ thicknesses over time and temperature. First, the thickening of the oxide scale and the OAZ is noticeably effective only during the first short dwell at 600 °C; the two following dwells at 535 °C and 525 °C appear to have only a small effect on the oxide scale growth. Second, when the temperature drops down significantly and quickly before stabilizing for a relatively long duration, the oxide scale is then slightly reduced before starting to regrow. This temporary reduction of the oxide is due to a change in the flux balance at the metal|oxide interface (Eq. (24)) when the temperature drops. A similar phenomenon was previously predicted and observed [25,29] on Zr alloys under particular conditions by Mazères *et al.* In Mazères's work, the conditions explored reproduced a hypothetical scenario of loss-of-coolant-accident affecting claddings of a pressurized water reactor, involving a fast temperature increase from 320 °C to 1 200 °C. In the case of Zr alloys, the partial reduction of the oxide scale was attributed to the fact that as temperature rises, the oxygen solubility in the metallic matrix increases as well.

In the present case of the Ti alloy, the phenomenon is not due to a change in solubility limit with temperature, but to a change in diffusion coefficients with temperature in both the oxide and the metal. Indeed,

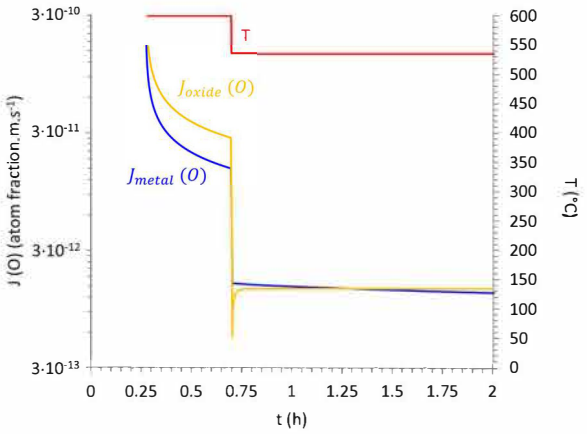

Fig. 12. Evolution of oxygen fluxes getting out of the oxide (orange) and getting into the metal (blue) as a function of time during the temperature transient from 600 °C to 535 °C. (For interpretation of the references to colour in this figure legend, the reader is referred to the web version of this article.)

the partial reduction of the oxide can be easily explained through the evolution of local oxygen fluxes $J^{TiO_2|Ti}_{O\,(ox)}$ and $J^{Ti|TiO_2}_{O\,(met)}$ on each side of the oxide|metal interface. Fig. 12 presents the evolution of these oxygen fluxes as a function of time during the temperature transient from 600 °C down to 535 °C. The activation energy of oxygen diffusion in the oxide ($G_{O\,(TiO_2)} = 243\,\text{kJ.mol}^{-1}$) is higher than in the metal ($G_{O\,(Ti)} = 203\,\text{kJ.mol}^{-1}$). This implies that the diffusion coefficient of oxygen in the oxide is more sensitive to temperature changes and therefore so is the associated oxygen flux in the oxide. In the present case, the quick temperature drop from 600 °C down to 535 °C causes the oxygen flux getting out of the oxide to be temporarily lower than the one getting into the metal. The oxygen flux in the oxide reaching the oxide|metal interface is then no longer sufficient to sustain oxygen diffusion in the metal. Considering the equilibrium conditions at the interface, this leads to a partial reduction of the oxide scale until the flux balance at the oxide|metal interface becomes positive again. Such a condition is progressively reached, because the O flux in the metal decreases with its concentration gradient, coupled with the O flux in the oxide that remains high, because of the very low growth of the oxide scale during the lower temperature dwells. The oxide scale then starts re-growing parabolically until any new thermal perturbation occurs.

As far as titanium oxidation is concerned, such a phenomenon has never been evidenced experimentally nor reported. However, the present calculations show that, under the conditions explored here, this phenomenon is rather insignificant. It is difficult to anticipate what it might imply in terms of mechanical degradation. This phenomenon could lead to the temporary formation of a saturated α-Ti(O) area between the oxide scale and the remaining metallic matrix. Formation of such a brittle phase, perhaps porous because it results from the reduction of an oxide phase, might noticeably affect the mechanical properties of the component, favoring crack initiation conditions already induced by the oxidation of the material.

Fig. 13 presents the evolution of mass gains per unit area over four consecutive thermal cycles. It indicates that the material behaviour is slightly different during the thermal cycles that follow the initial one, confirming the transient nature of the first cycle.

Fig. 14 presents the evolution of OAZ and oxide scale thicknesses as a function of the square root of the number of thermal cycles for 16 thermal cycles. According to Fig. 14, OAZ and oxide scale thicknesses evolution over time follow parabolic laws over the number of thermal cycles as long as the sample does not start to saturate in oxygen. The growth rate is much higher for the OAZ than for the oxide scale. The parabolic rate constants are respectively 0.97 $\mu\text{m.nb}_{\text{cycle}}^{-1/2}$ for the OAZ, and $9.0{\cdot}10^{-2}$ $\mu\text{m.nb}_{\text{cycle}}^{-1/2}$ for the oxide scale. For pratical purposes, it is

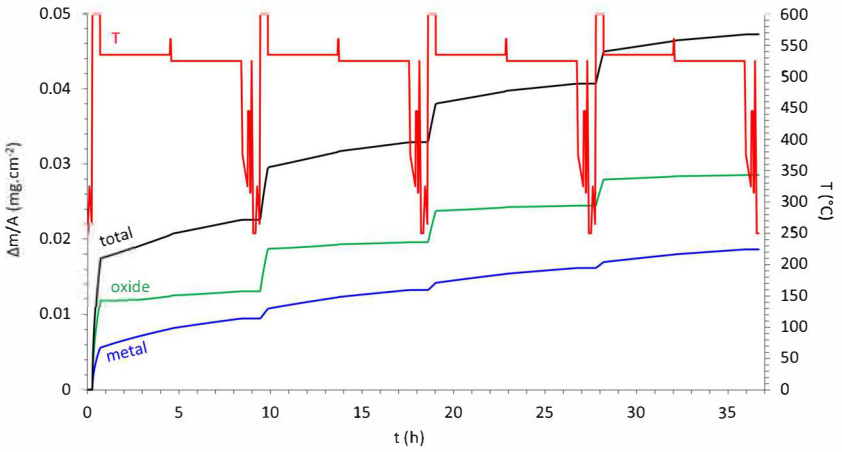

Fig. 13. Evolution of mass gains per unit area over time for 4 thermal cycles.

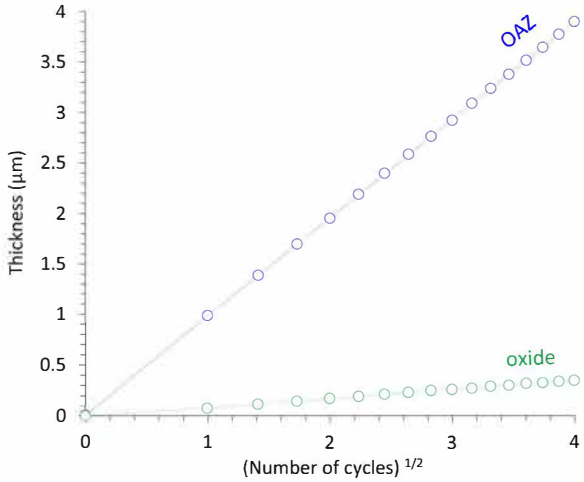

Fig. 14. Evolution of OAZ (blue) and oxide scale (green) thicknesses with the square root of the number of thermal cycles. (For interpretation of the references to colour in this figure legend, the reader is referred to the web version of this article.)

interesting to calculate the equivalent isothermal oxidation treatment that would give the same parabolic rate constants. This was applied to the present case; results show that an isothermal oxidation at a temperature of 538 °C would lead to the same OAZ growth rate and an isothermal oxidation at a temperature of 546 °C would lead to the same oxide scale growth rate. Again, these values show the important contribution of the short period at 600 °C over the entire cycle. Of course, all these considerations are only valid if the metallic matrix does not undergo any significant metallurgical evolution.

4. Conclusion

The aim of this work was to study the influence of different features on the high-temperature oxidation behavior of titanium alloys based on O diffusion modelling. A new 1D finite differences numerical model which includes boundary displacement, has been developed for Ti-alloys oxidation. The model's input parameters are the O diffusion coefficients in the alloy and in the Ti oxide phase, along with the equilibrium concentration at the oxide|gas and metal|oxide interfaces. Output data are: the oxygen concentration profiles in the two phases as well as the oxide growth and the metal recession.

For a given sample, it is therefore possible to calculate which proportion of its mass gain is attributable to oxide scale growth and which proportion is attributable to O diffusion in the matrix.

In the calculations carried out in this study, the input parameters were chosen in order to reproduce the literature-based experimental data obtained on Ti-6Al-2Sn-4Zr-2Mo-Si alloy. For this alloy, the Oxygen Affected Zone (OAZ) thickness, deduced from the O concentration profile calculations, was defined as the part of the alloy with over 0.5 at. % of O. This corresponds to the brittle region found in previous literature results. With this definition, it was possible to follow OAZ growth kinetics as a function of different parameters and oxidation conditions.

First, it is important to state that all calculations show that, even though O diffusion in the alloy only accounts for 30 % to 50 % of the total mass gain, the OAZ depth in the alloy is significantly thicker than the oxide scale. This is of major concern as far as embrittlement is concerned.

Second, the effect of nominal O concentration on the theoretical life span – when the latter is controlled by OAZ thickness – was deduced from analytical calculations for a typical wall thickness of 1 mm. It shows that depending on the nominal O concentration of the alloy batch, ranging from 0.15 at. % to 0.45 at. % (1 500 at. ppm to 4 500 at. ppm), the theoretical life span estimated from the OAZ depth in relation to the sample thickness, can be divided by two. The results also give an estimation of the life span's order of magnitude at in-service temperatures: typically, only one thousand hours at 650 °C to ten thousand hours at 500 °C.

Third, it was shown that the new numerical tool – PyTiOx – can overcome certain limitations relative to analytical models. The case of thin samples or thin parts is important, especially for additively manufactured components. Results from numerical models show that Pawel's model, which consists in a few modifications of Wagner's model that captures the treatment of finite size samples by analytical approximation, suffers from a lack of consistency. It does not reproduce correctly the coupling between oxide growth and O diffusion in the alloy once the O diffusion profile reaches the middle of the sample. In this case, the numerical model should be used. Through this method, it is possible to calculate the increase in oxide scale growth kinetics as the substrate becomes richer in oxygen.

Fourth, the numerical model was used to calculate the oxidation induced by a temperature transient similar to the conditions undergone by an aircraft engine component. Results show that the shortest time dwell, corresponding to the take-off stage, which is when the temperature is the highest, has the strongest effect on OAZ and oxide scale growth. However, calculations also revealed that the longer dwells corresponding to cruise stages cannot be completely neglected. Calculations over several cycles also confirmed that the OAZ thickness follows a parabolic evolution with the number of thermal cycles, the parabolic rate growth of the OAZ being about 10 times higher than that of the oxide scale in these conditions.

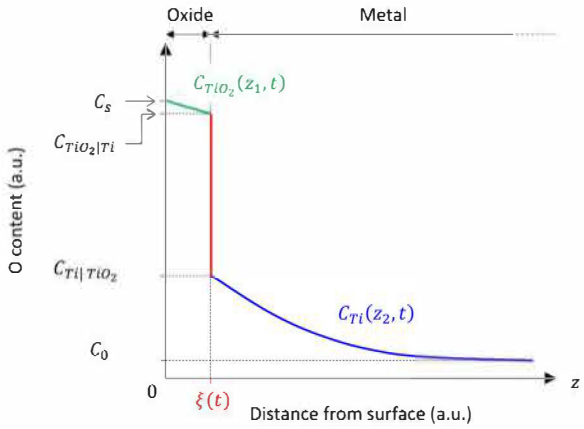

Fig. 15. Graphical illustration of Wagner's model.

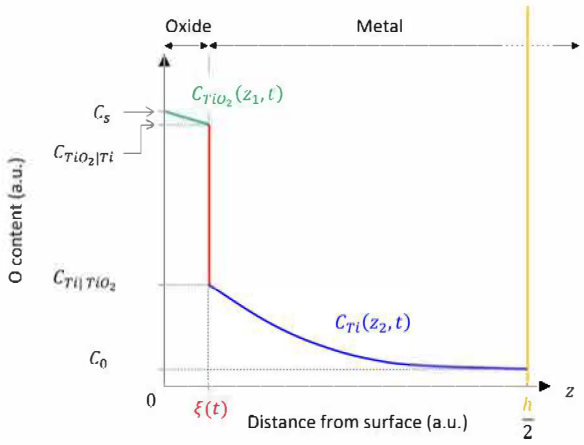

Fig. 16. Graphical illustration of Pawel's model.

Finally, an interesting phenomenon was brought to light during the thermal cycling. Because the activation energy of O diffusion is higher in the oxide than in the metal, it was shown that a drop in temperature results in a partial reduction of the oxide scale during a transient regime, before the scale regrows when the oxygen flux balance at the metal|oxide interface recovers the value corresponding to the new oxidation temperature. It would be interesting to investigate this effect experimentally. It has never been reported before and could impact mechanical proprieties. Numerical simulations could be used to define the conditions under which this phenomenon would be important.

The evolution of the microstructure of the $\alpha + \beta$ alloys with the O diffusion was completely neglected in the present calculations. This coupling might be of importance for some other Ti alloys and should therefore be investigated in the future with the PyTiOx model. In fact, with this numerical approach it is possible to solve diffusion equations with O diffusion coefficients that vary locally with the α/β phase ratio for example. In the present calculation, the oxide scale properties are held constant. The numerical approach used in the PyTiOx model could help integrate the well-known periodic layering of titanium oxides.

Data availability

The raw/processed data required to reproduce these findings cannot be shared at this time due to legal or ethical reasons.

CRediT authorship contribution statement

Clément Ciszak: Software, Validation, Data curation, Writing - original draft, Visualization. **Daniel Monceau:** Conceptualization, Methodology, Validation, Resources, Writing - review & editing, Supervision, Project administration, Funding acquisition. **Clara Desgranges:** Conceptualization, Methodology, Software, Validation, Resources, Writing - review & editing, Supervision, Project administration, Funding acquisition.

Declaration of Competing Interest

The authors report no declarations of interest.

Acknowledgements

This work was financially supported by the CIRIMAT laboratory and SAFRAN Tech. The authors thank Pierre-François BEHAGHEL from Safran Nacelles and Pierre DELALEAU from Safran Aircraft Engines for helpful discussions.

Appendix A

This section briefly presents the models of Wagner and Pawel. For more detailed information, for instance regarding the physical assumptions and calculation steps leading to the solutions of these two models, the reader is invited to refer directly to the work of Crank [5].

Description of Wagner's model

As oxide scale growth and oxygen dissolution are two correlated phenomena, Wagner [7] proposed an analytic model that can be used in a semi-infinite system to calculate oxygen diffusion profiles within the metal (Eqs. (3) and (4)) and the oxide growing on it (Eq. (2)). It also captures the displacement of the associated metal|oxide interface (Eq. (6)). Wagner's model assumes that the entire system is at thermodynamic equilibrium, i.e. all boundary conditions (C_s, $C_{TiO_2|Ti}$, $C_{Ti|TiO_2}$ and C_0) and diffusion coefficients ($D_{O\,(TiO_2)}$ and $D_{O\,(Ti)}$) are only temperature and pressure dependent. The coupling between oxide scale formation (diffusion and thickening) and diffusion within the metal is accounted by the constant γ. The value of the constant γ can be deduced from Eq. (7), which only depends on the physico-chemical parameters listed above. This constant γ is directly linked to the division of the oxygen flux reaching the metal|oxide interface: one part of the oxygen is dissolved in the alloy, while the other is involved in the growth of the oxide scale. Fig. 15 schematically summarizes the above description. The equations involved in Wagner's model are Eqs. (2)–(7).

Description of Pawel's model

Pawel's model [6] is based on the same assumptions as Wagner's with the same input parameters, i.e. all taken constant for a given temperature and pressure, except that the metal is of finite size and not semi-infinite. Fig. 16 schematically summarizes the above description. The modified solution proposed by Pawel to deal with diffusion within a finite medium, while taking into account the concomitant formation of a second phase growing from it, is represented by Eqs. (8) and (9).

Appendix B. Supplementary data

Supplementary material related to this article can be found, in the online version, at doi:https://doi.org/10.1016/j.corsci.2020.109005.

References

[1] P. Kwasniak, M. Muzyk, H. Garbacz, K.J. Kurzydlowski, Influence of oxygen content on the mechanical properties of hexagonal Ti—first principles calculations, Mater. Sci. Eng. A. 590 (2014) 74–79, https://doi.org/10.1016/j.msea.2013.10.004.

[2] H. Conrad, Effect of interstitial solutes on the strength and ductility of titanium, Prog. Mater. Sci. 26 (1981) 123–403, https://doi.org/10.1016/0079-6425(81)90001-3.

[3] B. Mazères, C. Desgranges, C. Toffolon-Masclet, D. Monceau, Contribution to modeling of hydrogen effect on oxygen diffusion in Zy-4 alloy during high temperature steam oxidation, Oxid. Met. 79 (2013) 121–133, https://doi.org/10.1007/s11085-012-9335-1.

[4] P. Kofstad, High Temperature Corrosion, Elsevier Applied Science, New York, USA, 1988.

[5] J. Crank, The Mathematics of Diffusion, 2nd ed., Clarendon Press, Oxford, 1975.

[6] R.E. Pawel, Diffusion in a finite system with a moving boundary, J. Nucl. Mater. 49 (1974) 281–290, https://doi.org/10.1016/0022-3115(74)90040-3.

[7] C. Wagner, W. Jost, Diffusion in Solids, Liquids, Gases, Diffus. Ed. Jost W. Academic Press N. Y., 1952, 1952 P. 71.

[8] P. Kofstad, Thermogravimetric studies of the defect structure of rutile (TiO_2), J. Phys. Chem. Solids 23 (1962) 1579–1586, https://doi.org/10.1016/0022-3697(62)90240-8.

[9] D.R. Lide, CRC Handbook of Chemistry and Physics, 90th ed., CRC Press, Boca Raton, 2009.

[10] Z. Liu, G. Welsch, Literature survey on diffusivities of oxygen, aluminum, and vanadium in Alpha Titanium, Beta titanium, and in rutile, Metall. Trans. A. 19 (1988) 1121–1125, https://doi.org/10.1007/BF02628396.

[11] R.N. Shenoy, J. Unnam, R.K. Clark, Oxidation and embrittlement of Ti-6Al-2Sn-4Zr-2Mo alloy, Oxid. Met. 26 (1986) 105–124, https://doi.org/10.1007/BF00664276.

[12] C.E. Shamblen, T.K. Redden, Air contamination and embrittlement of titanium alloys, in: R.I. Jaffee, N.E. Promisel (Eds.), Sci. Technol. Appl. Titan., Pergamon, 1970, pp. 199–208, https://doi.org/10.1016/B978-0-08-006564-9.50027-0.

[13] B. Mazères, C. Desgranges, C. Toffolon-Masclet, D. Monceau, Modeling two- and three-stage oxygen tracer experiments during high-temperature oxidation of metals with a high oxygen solubility, Oxid. Met. 89 (2018) 517–529, https://doi.org/10.1007/s11085-017-9816-3.

[14] H. Larsson, T. Jonsson, R. Naraghi, Y. Gong, R.C. Reed, J. Ågren, Oxidation of iron at 600 °C – experiments and simulations, Mater. Corros. 68 (2017) 133–142, https://doi.org/10.1002/maco.201508781.

[15] L. Bataillou, C. Desgranges, L. Martinelli, D. Monceau, Modelling of the effect of grain boundary diffusion on the oxidation of Ni-Cr alloys at high temperature, Corros. Sci. 136 (2018) 148–160, https://doi.org/10.1016/j.corsci.2018.03.001.

[16] A. Atkinson, R.I. Taylor, The self-diffusion of Ni in NiO and its relevance to the oxidation of Ni, J. Mater. Sci. 13 (1978) 427–432, https://doi.org/10.1007/BF00647789.

[17] C. Dupressoire, M. Descoins, A. Vande Put, D. Mangelinck, P. Emile, D. Monceau, The nitrogen effect on the oxidation behaviour of Ti6242S titanium-based alloy: contribution of atom probe tomography, in: The 14th World Conference on Titanium, Nantes, France, 2019.

[18] C. Dupressoire, Private Communication, 2020.

[19] Y. Millet, Private Communication, 2019.

[20] TIMETAL® 6-2-4-2 datasheet, https://www.timet.com/assets/local/documents/datasheets/alphaalloys/6242.pdf.

[21] C. Ciszak, D. Monceau, C. Desgranges, Modelling the high temperature oxidation of titanium alloys: review of analytical models and development of a new numerical tool PyTiOx, in: The 14th World Conference on Titanium, Nantes, France, 2019.

[22] F.C. Iglesias, D.B. Duncan, S. Sagat, H.E. Sills, Verification of the from model for zircaloy oxidation during high temperature transients, J. Nucl. Mater. 130 (1985) 36–44, https://doi.org/10.1016/0022-3115(85)90292-2.

[23] V.F. Strižov, Models for the Fuel Rod Materials Interactions During Reactor Core Degradation Under Server Accident Conditions at NPP, Nauka, Moskva, 2007.

[24] C. Duriez, S. Guilbert, A. Stern, C. Grandjean, L. Bělovský, J. Desquines, Characterization of oxygen distribution in LOCA situations, J. ASTM Int. 8 (2011) 1–19, https://doi.org/10.1520/JAI103156.

[25] B. Mazères, C. Desgranges, C. Toffolon-Masclet, D. Monceau, Experimental study and numerical simulation of high temperature (1100–1250 °C) oxidation of prior-oxidized zirconium alloy, Corros. Sci. 103 (2016) 10–19, https://doi.org/10.1016/j.corsci.2015.10.018.

[26] T. Kitashima, L.J. Liu, H. Murakami, Numerical analysis of oxygen transport in Alpha Titanium during isothermal oxidation, J. Electrochem. Soc. 160 (2013) C441–C444, https://doi.org/10.1149/2.100309jes.

[27] D. Monceau, Modélisation des phénomènes de ségrégation dynamique dans les céramiques conséquences sur l'élaboration des poudres et des monocristaux d'alumine-alpha dopée, thesis, Paris 13, 1992, http://www.theses.fr/1992PA132038.

[28] C. Desgranges, G. Martin, F. Defoort, Microstructural kinetics in alloys undergoing transmutations: application to Aic neutron absorbers, MRS Online Proc. Libr. Arch. 439 (1996), https://doi.org/10.1557/PROC-439-401.

[29] C. Toffolon-Masclet, C. Desgranges, C. Corvalan-Moya, J.C. Brachet, Simulation of the β→α(O) phase transformation due to oxygen diffusion during high temperature oxidation of zirconium alloys, Solid State Phenom. (2011), https://doi.org/10.4028/www.scientific.net/SSP.172-174.652.

[30] N. Bertrand, C. Desgranges, A. Terlain, D. Poquillon, D. Monceau, Numerical Model for Oxidation of Metallic Materials with Explicit Treatment of Cationic and Anionic Vacancy Fluxes, University of Aveiro, Portugal, 2005.

[31] C. Desgranges, N. Bertrand, K. Abbas, D. Monceau, D. Poquillon, Numerical model for oxide scale growth with explicit treatment of vacancy fluxes, Mater. Sci. Forum. 461–4 (2004) 481–488.

[32] N. Bertrand, C. Desgranges, M. Nastar, G. Girardin, D. Poquillon, D. Monceau, Chemical evolution in the substrate due to oxidation: a numerical model with explicit treatment of vacancy fluxes, Mater. Sci. Forum. 595–5 (2008) 463–472.

[33] H. Larsson, R.C. Reed, On the numerical simulation of diffusion-controlled reactions under local equilibrium conditions, Acta Mater. 56 (2008) 3754–3760, https://doi.org/10.1016/j.actamat.2008.04.008.

[34] A. Finel, Y. Le Bouar, B. Dabas, B. Appolaire, Y. Yamada, T. Mohri, Sharp phase field method, Phys. Rev. Lett. 121 (2018), 025501, https://doi.org/10.1103/PhysRevLett.121.025501.